

The role and effect of CO₂ flow rate on the structure formation of ultrahigh porous activated carbon from H₃PO₄-impregnated waste cotton used as supercapacitor electrode material

Nguyen K. Thach^{1,2,a}, Ilya S. Krechetov^{1,b}, Valentin V. Berestov^{1,c}, Oleg I. Kan^{1,d},
Ivan A. Maslochenko^{1,e}, Tatyana L. Lepkova^{1,f}, Svetlana V. Stakhanova^{1,3,g}

¹National University of Science and Technology “MISIS”, Moscow, Russia

²College of electromechanical and civil engineering, Vietnam National University of Forestry, Hanoi, Vietnam

³Mendeleev University of Chemical Technology of Russia, Moscow, Russia

^anguyenkienthach@gmail.com, ^bilya.krechetov@misis.ru, ^cvberestov97@gmail.com, ^dm2106915@edu.misis.ru,

^emaslochenko3@mail.ru, ^flepkova.tl@misis.ru, ^gstakhanova.s.v@muctr.ru

Corresponding author: N. K. Thach, nguyenkienthach@gmail.com

ABSTRACT Ultrahigh porosity activated carbon (AC) was made from H₃PO₄-impregnated waste cotton precursor by carbonization in Ar and physical activation in variable CO₂ flow rate with ultrahigh heating rate. The presence of CO₂ in the activation plays an important role in the formation of the porous structure of AC. The obtained AC had outstanding physical and electrochemical properties. The specific surface area and micropore volume of AC reached 4800.7 m²/g and 2.499 cm³/g, respectively. The pore size distribution was mainly in the microporous region. The electrochemical double-layer capacitors (EDLCs) with AC-based active electrode and an electrolyte solution of 1 M 1,1-dimethylpyrrolidinium tetrafluoroborate in acetonitrile were fabricated. The specific capacitance of electrode material degraded less than 10 % with the highest value of 105.7 F/g at 0.05 A/g as the specific current varied from 0.05 A/g – 15 A/g. After 8000 charge-discharge cycles at 1 A/g, the specific capacitance of the AC-base electrode material fabricated at CO₂ flow rate greater than 200 ml/min degraded less than 15 % with the highest value of 101.2 F/g. The optimal CO₂ flow rate for fabricating waste cotton-based AC is 200 ml/min.

KEYWORDS activated carbon, porous activated carbon, cellulose, waste cotton, supercapacitor.

ACKNOWLEDGEMENTS The authors would like to thank Dr. Alexey Igorevich Salimon, Dean of the Department of Physical Chemistry, the College of New Materials and Nanotechnologies, the University of Science and Technology “MISIS”, Moscow, Russia, for valuable recommendations on the content of the article. The authors would also like to thank The Hierarchically Structured Materials Lab, Center for Digital Engineering, Skoltech, Moscow, Russia, for helping us to conduct the BET and SEM measurements.

FOR CITATION Thach N.K., Krechetov I.S., Berestov V.V., Kan O.I., Maslochenko I.A., Lepkova T.L., Stakhanova S.V. The role and effect of CO₂ flow rate on the structure formation of ultrahigh porous activated carbon from H₃PO₄-impregnated waste cotton used as supercapacitor electrode material. *Nanosystems: Phys. Chem. Math.*, 2023, **14** (4), 489–497.

1. Introduction

Energy has been the crucial issue for the global economy. Currently, the main energy resources for human are fossil resources such as coal, crude oil, and natural gas, etc. The excessive use and depletion of these resources have been causing serious environmental pollution. Therefore, people have been looking for renewable energy sources that are environmentally friendly and can gradually replace fossil fuels such as solar energy, wind energy, tidal energy [1–3], etc. However, these energy sources are intermittent and vary with time of a day, seasons, and years. So, they have been required a highly efficient energy storage and conversion system to maintain continuous operation. Batteries and supercapacitors are main electrical energy storage and conversion devices today.

Batteries store energy in the form of chemical energy based on redox reactions occurring on the electrodes. The stored energy of the battery is large and can meet most of the energy demands of electrical and electronic devices in daily life [4]. The drawbacks of the batteries are low power density, short life-cycle and containing some toxic substances that are harmful to the environment at the end of their life. Meanwhile, EDLCs store energy in the form of static electricity that is formed on the interface of the electrochemical double layer between the electrolyte solution and the electrode material surface [5]. Comparing to batteries, EDLCs have a much lower energy density but have higher power density, energy conversion efficiency, long life-cycle (over 100000 charge-discharge cycles) and can operate in extreme environments

with temperatures ranging from $-40 - +75$ °C [1, 5]. Therefore, depending on the real life applications, batteries and supercapacitors have been used as stand-alone systems or integrated both into real devices such as lights, maintain and protect the memory of electronic devices, cars, trains, and space devices [6, 7], etc. to take benefit of their advantages and limit their drawbacks.

Recently, high porosity AC (with specific surface area greater than 1000 m²/g) has been widely used as electrode materials for both batteries and supercapacitors. Among the materials used to produce porous AC, biomass materials are receiving much attention from researchers because they are available, abundant, renewable, and environmentally friendly. They are often waste products of the agricultural and forest products processing industry such as rice husks [8], corncob [9], olive stones [10], sugarcane bagasse [11], cotton [12–14], and cotton stalk [15], etc. To convert biomass materials into porous AC, two main processes are used: carbonization and activation.

The carbonization process is usually carried out in an inert gas (N₂ or Ar) at temperatures between 400 and 900 °C. The precursors have been impregnated with substances such as ZnCl₂ [16], KOH, H₃PO₄ [11, 17], etc. with different ratios to increase the carbon yield of the obtained products and create favorable conditions for the growth of pore structures during the activation process. There are two processes of carbon activation: physical activation and chemical activation. The physical activation is carried out in a redox gaseous environment such as CO₂, H₂O [18], etc at a temperature of $700 - 1200$ °C. These redox gases diffuse deep into the structure of carbon and react with carbon to form and expand pore structures. As a result, the obtained porous AC has large surface area and good pore size distribution. Meanwhile, chemical activation is carried out at a temperature of $500 - 800$ °C in the presence of activating agents. The raw material is impregnated with a given activating agent and there are many selective chemical reactions occurring during activation. The result is AC with an amorphous material and the existence of intercalate ions in the structure.

In this study, H₃PO₄-impregnated waste cotton was used to fabricate porous AC because cotton is a naturally highly porous, high content of cellulose (between $80-97\%$ by weight [15, 19, 20]) and less impurities. The porous AC production was conducted in two processes: carbonization at 600 °C in Ar atmosphere and activation at 900 °C in the absence or presence of CO₂ with variable gas flow rate.

2. Materials and methods

2.1. Fabricating porous AC

2.1.1. Preparing H₃PO₄-impregnated waste cotton. Waste cotton was supplied by Yartsevo Cotton Mill, LLC (Russia).

85% H₃PO₄ solution according to standard GOST 6552-80 (Russia) was diluted with deionized water to form 5% H₃PO₄ solution.

20 g of cotton was immersed in 600 g of 5% H₃PO₄ solution. The mixture was heated to a temperature above 80 °C and maintained for 30 minutes. The cotton was then squeezed out and dried at room temperature for 48 h.

2.1.2. Carbonization process. Based on our previous research results on optimizing the temperature of the carbonization process to the properties of activated carbon used as electrode materials for supercapacitors [21], we choose the temperature of 600 °C to conduct the carbonization process of H₃PO₄-impregnated cotton.

To increase the uniformity of the torn cotton compared to our previous experiments, 5 g of H₃PO₄-impregnated cotton was torn up by the tearing machine and then loaded into a horizontal reaction chamber with a length of 60 cm and a diameter of 10 cm. Then, Ar gas was supplied at a flow rate of 800 ml/min for 10 minutes to remove air.

Initially, the furnace was heated to 600 °C with a heating rate of 10 °C/min. After reaching the temperature of 600 °C, the reaction chamber was loaded into furnace and maintained with a flow rate of Ar gas of 800 ml/min. By this method, the heating rate of 585 °C/min $\pm 10\%$ was achieved. The carbonization time was 1 h. After carbonization, the reaction chamber was taken out and cooled to room temperature with an Ar flow rate of 800 ml/min and a cooling system. The product was called black carbon fiber (BCF). The obtained products were weighed and stored in nylon bags to avoid dust.

2.1.3. Activation process. 1.5 g BCF was added into the reaction chamber. The Ar gas was supplied at a flow rate of 800 ml/min for 10 minutes to remove air.

Initially, the furnace was heated to 900 °C with a heating rate of 10 °C/min. When the furnace reached 900 °C, the reactor chamber was loaded inside, and an Ar flow rate of 800 ml/min was maintained. The heating rate of 751 °C/min $\pm 10\%$ was achieved. When the system was reached 900 °C again, the Ar supply was cut off and CO₂ was supplied with a flow rate varying from $100 - 800$ ml/min. The activation time was 1 h. When the activation process was complete, the CO₂ flow was cut off and the reaction chamber was taken out and cooled to room temperature with an Ar flow rate of 800 ml/min and a cooling system. The obtained AC products were labeled as CT0 to sample without CO₂, and CT1, CT2, CT4, CT8 corresponding to samples with CO₂ flow rate of $100, 200, 400$ and 800 ml/min. With the CT0 sample, the Ar flow rate of 100 ml/min was maintained to remove volatile derivatives during activation.

2.2. Fabricating supercapacitor

2.2.1. Fabricating carbon electrode. The AC was crushed by mortar and mixed with polytetrafluoroethylene F4D suspension (Russia) used as the binder and carbon black (CABOT®VULCAN ©XC72) as the conducting agent according to the ratio percentage by mass was 80:10:10. The mixture was then added in a glass flask containing 100 ml of deionized water and stirred at 50 °C for 30 minutes. The slurry was filtered, and the obtained material was rolled on a mechanical roller to form a thin film with a thickness of 150 μm. The films were then cut into square electrodes with dimensions of 2.5×2.5 cm and dried at 120 °C in drying oven for 24 h and weighed to an accuracy of 0.001 g.

2.2.2. Fabricating supercapacitor. Two carbon electrodes were selected as active electrodes of a capacitor with a mass difference of less than 0.002 g. These carbon electrodes were pasted on the aluminum foils (OKURA-801, Japan) by RIKON adhesive (Russia). Two complete electrodes were placed opposite and separated by separator TF-40-30 (Japan). The electrode system was placed in an adhesive enclosure and kept under vacuum at 120 °C for 48 h. Next, the enclosure was filled with 1 ml electrolyte solution of 1M 1,1-dimethylpyrrolidinium tetrafluoroborate (DMP·BF₄) in acetonitrile (ACN) solvent and packed to form a complete capacitor.

2.3. Instruments and methods for investigating physical and electrochemical properties of porous AC

The surface morphology of AC was investigated by the scanning electron microscope (SEM) TESCAN MIRA (Czech).

The texture characteristics of AC were investigated by the N₂ adsorption-desorption method at 77 K on the Quantachrome LX² machine (Quantachrome, Austria).

X-ray diffraction (XRD) spectra were investigated on XPERT-PRO (Latvia) with the emission spectrum of copper with wavelength Kα = 1.541 Å. The X-ray scanning angle from 5 to 80 ° with a scan step of 0.03 ° and a dwelling time of 0.5 s.

The P20-X potentiostat (Elins, Russia) was used to measure the cyclic voltammetry (CV) characteristics of the supercapacitors.

The galvanostatic charge-discharge (GCD) method was used to test the performance of the supercapacitors by using ASK2.5.10.8 HIT analyzer (Russia).

3. Results and discussion

3.1. AC yield

According to K. Raveendran et al. [22], the thermal decomposition of cellulose and its derivatives takes place intensely in the temperature range of 350 – 450 °C. By the above carbonization method, the lowest furnace average temperature was reached 555 °C which was much greater than the thermal decomposition temperature range of cellulose. At this temperature, the thermal decomposition of cellulose takes place intensely. The decomposition products are water, CO₂, volatile compounds that exist in the gaseous state. These substances partially penetrate the cotton fiber to dissolve and break the structure of the cellulose crystals creating micro-swelling and the rest evaporate intensely. As a result, there is the formation of open or sealed porous structures that exist manifold within the structure of the obtained material. The carbon yield in our study was achieved average value of 32.3 %.

According to Peng Fu et al. [23], there are some heavy chemical compounds which exist in the solid carbon structure after carbonization and continue thermal decomposition at temperatures range 500 – 800°C. Therefore, there were some derivatives of the cellulose decomposition existing in the obtained BCF after carbonization. Furthermore, there were a certain amount of water vapor and gases which were adsorbed into BCF structure during the storage. Our carbon activation method described above was achieved the lowest furnace average temperature of 786 °C. At this temperature, the derivatives and gases adsorbed on the surface of BCF were evaporated and ejected by the Ar flow. This created favorable conditions for the contact of CO₂ with BCF surface during the activation and facilitated the formation of porous structures. The main reaction took place in the activation according to the equation CO₂ + C = 2CO. The AC yield was shown in Fig. 1.

As shown in Fig. 1, the AC yield decreased as increasing CO₂ flow rate. With sample CT0, the mass of the obtained AC was decreased when compared with the initial mass of BCF although no CO₂ was used in the activation process. This meant that some cellulose derivatives still existed in the original BCF after carbonization. For the other samples, the presence of CO₂ reacted with the carbon and significantly reduced the mass of the AC. The AC yield decreased as the CO₂ flow rate increased. This indicated that CO₂ burned most of the carbon and drastically reduced the AC yield at a high CO₂ flow rate.

When comparing the CT8 sample with the SP600 sample of the previous study [21] with the same flow rates of Ar and CO₂ for both carbonization and carbon activation processes, we found that the carbon yield after carbonization increase insignificantly (from 31.4% to 32.3%), while the activated carbon yield decreased significantly (from 3.3% to 2.2%). This shows that increasing the uniformity of the cotton before loading into the reaction chamber has increased the contact between the gas environment (Ar, CO₂) and the surface of the bulk cotton. As a result, in the carbonization, the

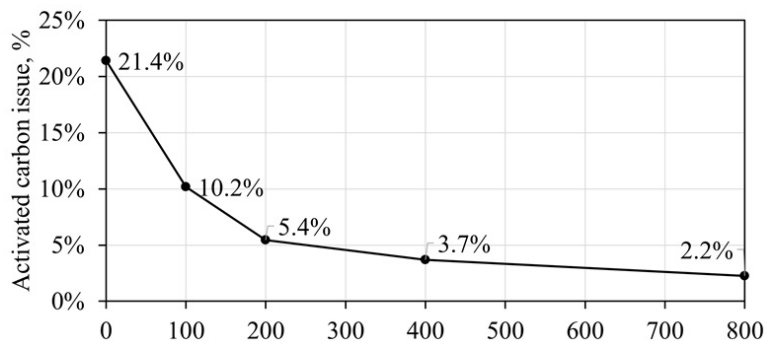


FIG. 1. Activated carbon yield after activation in the absence and presence of CO_2 at different flow rates

pyrolysis products of cotton will come out easily, the BCF fibers are not sticky. This increases the diffusion ability of CO_2 during activation into the BCF bulk, increasing the reaction between CO_2 and carbon leading to the decreasing activated carbon yield.

3.2. Physical properties of porous AC

The XRD spectrum of the AC samples were shown in Fig. 2. A broad (002) graphite plane peak at $2\theta \sim 23.8^\circ$ of sample CT0 was clearer than that of the other samples. This indicated that the CT0 sample was began to graphitize at 900°C while the rest samples were not. This evidence also demonstrated that CO_2 reacted with C on the pore wall, destroying the carbon crystal structure and increasing the amorphousness of the obtained porous AC. No obvious (001) graphite plane peak was observed at $2\theta \sim 44^\circ$. As a result, the AC was amorphous carbon.

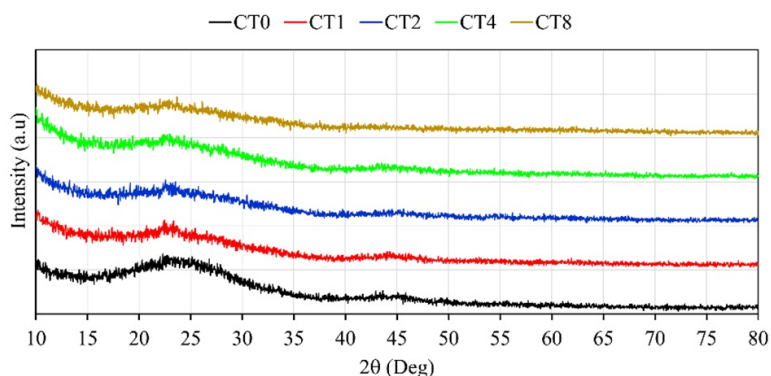


FIG. 2. XRD spectrum of the AC samples fabricated by activation with variable CO_2 flow rate

The SEM image of the CT2 sample was shown in Fig. 3. As shown in Fig. 3a,b, the obtained AC fiber retained the typical twisted, flattened shape of the original cotton fiber, without impurities adhering to the fiber surface and the fiber size was less than $10\ \mu\text{m}$. Fig. 3c showed that there was uniform pore formation, well development of pore structure and pore distribution in the microporous and mesoporous regions.

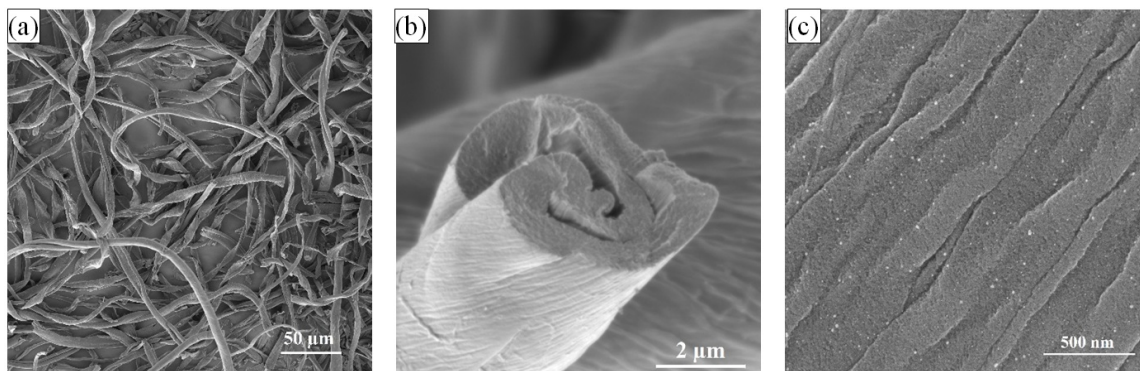


FIG. 3. SEM image of sample CT2

TABLE 1. The surface characteristics of the AC samples

Sample	S_{BET} (m ² /g)	S_{mic} (m ² /g)	S_{mes} (m ² /g)	V_{mic} (cm ³ /g)	d (nm)
CT0	651.2	–	–	0.343	0.52
CT1	1904.4	1220.3	684.1	0.869	1.32
CT2	4800.7	3138.8	1661.9	2.499	1.65
CT4	3557.8	2156.8	1401.0	1.963	1.98
CT8	3863.5	2460.2	1403.3	2.127	1.87

The N₂ adsorption-desorption method at the temperature of 77 K was used to investigate the surface characteristics of the porous AC. The degas process was conducted at 250 °C within 4 h in vacuum. The N₂ adsorption isotherms was conducted with the relative pressure (p/p_0) from 0.05 to 0.99 and obtained results as shown in Fig. 4. The N₂ isotherms of all samples had the form corresponding to Type I(b) according to the IUPAC classification [24, 25]. This meant that the pore size was mainly in the microporous region and partly in the mesoporous region with the size less than 2.5 nm. The N₂ adsorption capacity increased rapidly in the presence of CO₂ during the activation process and achieved the highest value at the CO₂ flow rate of 200 ml/min.

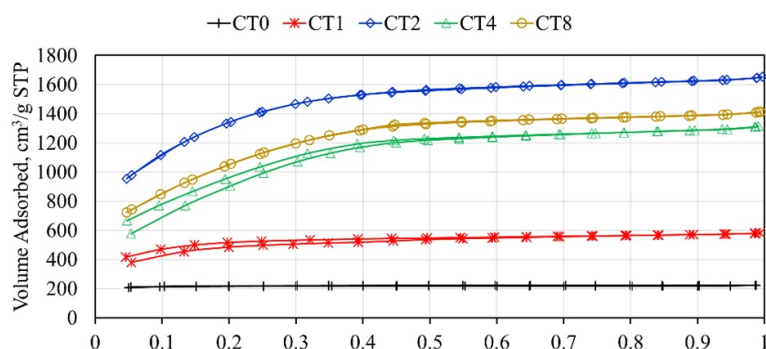


FIG. 4. N₂ adsorption-desorption isotherms of AC prepared in the absence or presence of CO₂ at different CO₂ flow rates

The Brunauer, Emmet, and Teller (BET) method was used to assess the specific surface area of the AC. The specific surface area (S_{BET}) was determined in the relative pressure range from 0.05 to 0.3 for the CT0 sample and 0.05 to 0.15 for the rest samples according to IUPAC recommendations for specific surface area assessment of microporous materials. The micropore volume (V_{mic}) and pore size (d) were determined by the Dubinin–Radushkevich (DR) method. The surface area of the micropore (S_{mic}) and pore size distribution were determined by the Density functional theory (DFT) method. The surface area of the mesopore (S_{mes}) is the result of the subtraction between S_{BET} and S_{mic} . The results were shown in Tables 1 and Fig. 5.

As shown in Table 1, specific surface area (S_{BET}), micropore surface area and micropore volume (V_{mic}) increased rapidly when the CO₂ flow rate increased from 0 to 200 ml/min and then decreased unevenly when the CO₂ flow rate increased from 200 to 800 ml/min. The highest values of S_{BET} , S_{mic} , and V_{mic} achieved at the CO₂ flow rate of 200 ml/min were 4800.7 m²/g, 3138.8 m²/g, and 2.499 cm³/g, respectively. This proved that the porous structures developed very well inside the initial BCF and facilitated the development of micropores during activation in the presence of CO₂. At low CO₂ flow rates, CO₂ molecules have enough time to diffuse deep into the structure of BCF and react with the carbon on the micropore wall to open and enlarge the pores, and thus increase specific surface area, micropore surface area and micropore volume. Meanwhile at high CO₂ flow rates, the amount of CO₂ is larger, the CO₂ molecules move faster and directly participates in the reaction with carbon on the micropore wall on the outer side of BCF more. Consequently, the S_{BET} , S_{mic} and V_{mic} decrease, and pore size is larger.

As shown in Fig. 5, the pore size distribution peaks of all samples located in the microporous region less than 2 nm and there are no peaks in the mesoporous region. The samples CT0, CT1 had low peaks and small micropore volume. Meanwhile, samples CT2, CT4, and CT8 had three outstandingly high main peaks and were in the microporous region with size less than 1.5 nm. Fig. 5 also showed that there was a shift of the pore size distribution peaks to a larger pore size region as the CO₂ flow rate increased from 200 to 800 ml/min.

When comparing the physical properties of sample CT8 with SP600 of the previous study [21], the obtained activated carbon has an amorphous structure in both cases. However, the specific surface area of the CT8 increased by about 40%

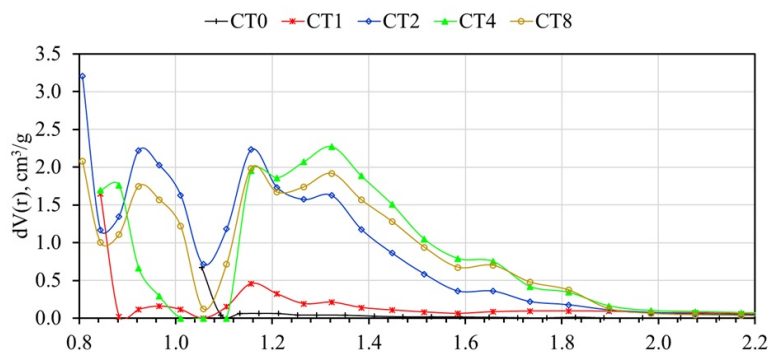


FIG. 5. Pore size distribution of AC materials was determined by the DFT method

compared with that of the SP600 while the pore size decreased from 2.62 nm to 1.87 nm. This again proves that increasing the uniformity of the initial torn impregnated cotton has increased the contact area and increased the diffusivity of CO_2 into the structure of BCF. Consequently, obtained activated carbon has outstanding physical properties.

3.3. Electrochemical properties of porous AC

There are many factors that affect the performance and capacitance of an EDLC such as electrolyte solution, carbon electrodes, collectors, binder [26], etc. Among others, the carbon electrodes and electrolyte solution are the two main factors affecting the performance and specific capacitance value of the EDLCs. The electrolyte adsorption capacity of porous AC materials depends on the surface area and surface functional groups when the carbon electrodes expose to an electrolyte solution. Besides, the matching of the pore size of AC and the electrolyte ion size plays an important role in the diffusion of electrolyte ions deep into the porous structure of carbon electrodes. The electrolyte ions in solution exist in a solvated state when combined with solvent molecules. In ACN solvent, the size of the $[\text{BF}_4]^-$ ion is about 1.40 nm while the bare ion size is 0.48 nm [27], and the $[\text{DMP}]^+$ ion has a bare size of 0.44 nm [28]. For microporous AC, when micropore size close to electrolyte ion size, electrolyte ions partly remove the solvent molecular shell and may be deformed during diffusion into micropores [28]. In contrast, the pores will also be deformed during the diffusion of these ions. Consequently, the specific capacitance of the electrode material will change during the continuous operation of the EDLCs.

Figure 6 showed the CV curves of the EDLCs at the potential scan rate of 100 mV/s with the potential varying from 0 to 2.7 V. The CV curve of CT0 was small and highly distorted, while the CV curves of CT1, CT2, CT4, CT8 were a like-rectangular shape. This demonstrated that the surface adsorption property of CT0's carbon electrodes are poor for $[\text{DMP}]^+$ and $[\text{BF}_4]^-$ ions. Meanwhile, the CT1, CT2, CT4, CT8 samples had the characteristics of the ideal capacitors, and their carbon electrodes had good reversible electrochemical properties.

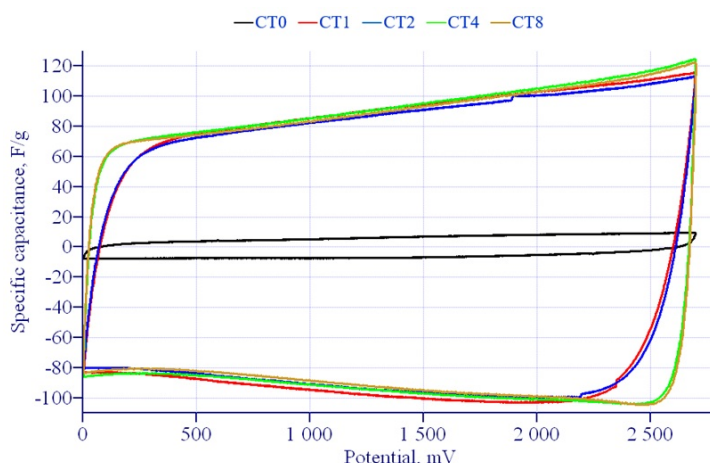


FIG. 6. The CV curves of fabricated supercapacitors at potential scan rate 100 mV/s

Figure 7 showed the dependence of the specific capacitance of electrode material of EDLCs depending on the specific current density varying from 0.05 A/g to 15 A/g and the charge-discharge characteristic of EDLCs at current density of 1 A/g. The specific capacitance of electrode material of CT0 sample was small and decreased quickly with increasing current density up to a value of 10 A/g. Besides, the GCD curve of the CT0 capacitor was asymmetrical and had large IR

drop (Fig. 7b). Therefore, the electrode material of the CT0 capacitor had poor reversibility electrochemical properties and was not suitable as an electrode material for EDLCs. In contrast, the specific capacitance of electrode material of CT1, CT2, CT4, CT8 capacitors were high and degrade less than 10 % as the current density increased up to a value of 15 A/g, and the GCD curves were highly symmetric, and small IR drop. The highest specific capacitance of electrode material reached 105.7 F/g for the CT₄ sample at 0.05 A/g. These proved that the obtained AC when using CO₂ in activation had high stability during the performance of the capacitors, good reversible electrolyte ions adsorption characteristics. The AC materials can be used as electrode materials for high-performance supercapacitors.

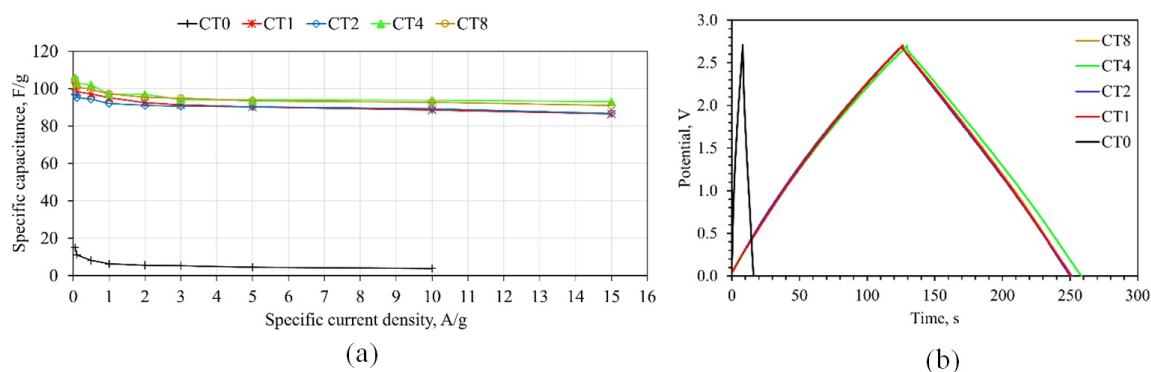


FIG. 7. (a) The dependence of specific capacitance on the current density from 0.05 A/g to 15 A/g and (b) the GCD curves at 1 A/g of the fabricated supercapacitors

When considering the surface area and pore size of AC (Table 1) affect the specific capacitance of electrode material, we found that although S_{BET} , S_{mic} varied greatly, the capacitance of the electrode material did not change much (ca. 5%) between samples CT1, CT2, CT4 and CT8. For the CT2 sample, S_{BET} , S_{mic} were much larger than that of the CT1 sample, but the pore size was mainly distributed in the ultra microporous region, so the electrolyte ions cannot access the inner surface of the pores. Thus, the specific capacitance value of CT2 and CT1 was the same value. The CT4 and CT8 samples had larger pore sizes and thus accessible electrolyte ions had a larger specific capacitance. This demonstrated that the specific capacitance of electrode material depended mainly on the pore size distribution rather than the specific surface area.

The GCD method was used to investigate the life-cycle of the supercapacitors with AC-based electrodes at current density of 1 A/g with potential varied from 0 to 2.7 V and 8000 charge-discharge cycles. We did not conduct GCD testing with the CT0 sample because it was unstable at 1 A/g. The GCD curves of the CT1, CT2, CT4 and CT8 were shown in Fig. 8.

As shown in Fig. 8, the relative capacitance of all capacitors changed rapidly (ca. 10%) during the first 1000 cycles. The CT1 sample was disconnected from the power supply after 4200 cycles. Then it was resumed operation, its relative capacitance recovered a significant value of ca. 90 % and degraded ca. 25% after 8000 cycles. Meanwhile, the specific capacitance of CT2, CT4 and CT8 degraded insignificantly (ca. 5%) from 1000 to 8000 cycles. The capacitance degradation of the CT2, CT4 and CT8 after 8000 cycles were 15%, 15 %, 12 %, respectively. The maximum capacitance value was achieved 101.2 F/g for the CT4 sample. Thus, the obtained activated carbon from activation with CO₂ flow rate greater than 200 ml/min exhibited more stability during the continuous operation of the EDLCs.

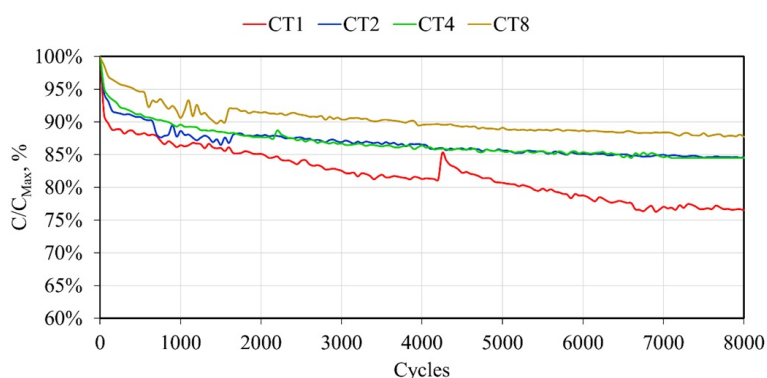


FIG. 8. The dependence of relative capacitance of supercapacitors on the number of charge-discharge cycles at a specific current density of 1 A/g and potential varied from 0 – 2.7 V

4. Conclusion

By carbonization method with extremely heating rate and the temperature of carbonization of H_3PO_4 -impregnated waste cotton much higher than that of cellulose, the BCF with abundance of sealed pores inside fiber structure was fabricated. The presence of CO_2 during the activation with extremely heating rate plays an important role in opening the sealed pores inside BCF structure and facilitating the growth of micropores. The obtained AC was the amorphous carbon and had ultrahigh specific surface area, micropore surface area and micropore volume of $4800.8 \text{ m}^2/\text{g}$, $3138.8 \text{ m}^2/\text{g}$ and $2.499 \text{ cm}^3/\text{g}$, respectively and the pore size distribution was mainly in the microporous region.

The EDLCs with carbon electrodes fabricated from AC obtained by activation in the presence of CO_2 have high stability and good reversible electrochemical properties to current density up to a value of 15 A/g , and the specific capacitance degradation of less than 10% . The specific capacitance degraded less than 15% with the samples that fabricated at CO_2 flow rate higher than 200 ml/min . The specific capacitance of activated carbon depends strongly on the matching of the average micropore size of AC material and the electrolyte ion size rather than the specific surface area of the material. While the surface area varies greatly and the pore size varies slightly, the specific capacitance of the electrode material changes insignificant. The obtained porous activated carbon material can be used as an electrode material for high-performance supercapacitors. We recommend that the CO_2 flow rate in the production of activated carbon from H_3PO_4 -impregnated waste cotton is 200 ml/min .

References

- [1] Şahin M., Blaabjerg F., and Sangwongwanich A. A Comprehensive Review on Supercapacitor Applications and Developments. *Energies (Basel)*, 2022, **15**(3), P. 674–699.
- [2] Kumar G.V.B., Kaliannan P., Padmanaban S., Holm-Nielsen J.B., and Blaabjerg F. Effective Management System for Solar PV Using Real-Time Data with Hybrid Energy Storage System. *Applied Sciences*, 2020, **10**(3), P. 1108–1122.
- [3] Yang Y., Han Y., Jiang W., Zhang Y., Xu Y., and Ahmed A.M. Application of the Supercapacitor for Energy Storage in China: Role and Strategy. *Applied Sciences*, 2021, **12**(1), P. 354–372.
- [4] Winter M., Brodd R.J. What Are Batteries, Fuel Cells, and Supercapacitors? *Chem Rev*, 2004, **104**(10), P. 4245–4270.
- [5] Kötzt R. and Carlen M. Principles and applications of electrochemical capacitors. *Electrochim Acta*, 2000, **45**(15–16), P. 2483–2498.
- [6] Burke A. Ultracapacitors: why, how, and where is the technology. *J. Power Sources*, 2000, **91**(1), P. 37–50.
- [7] Miller J.R. and Burke A. Electrochemical Capacitors: Challenges and Opportunities for Real-World Applications. *Electrochem Soc Interface*, 2008, **17**(1), P. 53–57.
- [8] Luo Y., Li D., Chen Y., Sun X., Cao Q., and Liu X. The performance of phosphoric acid in the preparation of activated carbon-containing phosphorus species from rice husk residue. *J. Mater. Sci.*, 2019, **54**(6), P. 5008–5021.
- [9] Sych N.V., et al. Porous structure and surface chemistry of phosphoric acid activated carbon from corncob. *Appl. Surf. Sci.*, 2012, **261**, P. 75–82.
- [10] Yakout S.M. and Sharaf El-Deen G. Characterization of activated carbon prepared by phosphoric acid activation of olive stones. *Arabian Journal of Chemistry*, 2016, **9**, P. S1155–S1162.
- [11] Adib M.R.M., et al. Effect of Phosphoric Acid Concentration on the Characteristics of Sugarcane Bagasse Activated Carbon. *IOP Conf. Ser. Mater. Sci. Eng.*, 2016, **136**, P. 012061–012069.
- [12] Nahil M.A. and Williams P.T. Characterisation of Activated Carbons with High Surface Area and Variable Porosity Produced from Agricultural Cotton Waste by Chemical Activation and Co-activation. *Waste Biomass Valorization*, 2012, **3**(2), P. 117–130.
- [13] Sartova K., Omurzak E., Kambarova G., Dzharmaev I., Borkoev B., and Abdullaeva Z. Activated carbon obtained from the cotton processing wastes. *Diam. Relat. Mater.*, 2019, **91**, P. 90–97.
- [14] Ma G. et al. Cotton-based porous activated carbon with a large specific surface area as an electrode material for high-performance supercapacitors. *RSC Adv.*, 2015, **5**(79), P. 64704–64710.
- [15] Nahil M.A. and Williams P.T. Pore characteristics of activated carbons from the phosphoric acid chemical activation of cotton stalks. *Biomass Bioenergy*, 2012, **37**, P. 142–149.
- [16] Liou T.-H. Development of mesoporous structure and high adsorption capacity of biomass-based activated carbon by phosphoric acid and zinc chloride activation. *Chemical Engineering Journal*, 2009, **158**, **2**, P. 129–142.
- [17] Xia M., Shao X., Sun Z., and Xu Z. Conversion of cotton textile wastes into porous carbons by chemical activation with ZnCl_2 , H_3PO_4 , and FeCl_3 . *Environmental Science and Pollution Research*, 2020, **27**(20), P. 25186–25196.
- [18] Budinova T. et al. Characterization and application of activated carbon produced by H_3PO_4 and water vapor activation. *Fuel Processing Technology*, 2006, **87**(10), P. 899–905.
- [19] Ma G. et al. Cotton-based porous activated carbon with a large specific surface area as an electrode material for high-performance supercapacitors. *RSC Adv.*, 2015, **5**(79), P. 64704–64710.
- [20] Wakelyn P.J. *Cotton Fiber Chemistry and Technology*. CRC Press, 2006.
- [21] Thach N.K., Krechetov I.S., Berestov V.V., Lepkova T.L., and Stakhanova S.V. Optimizing the carbonization temperature in the fabrication of waste cotton based activated carbon used as electrode material for supercapacitor. *Nanosystems: Physics, Chemistry, Mathematics*, 2022, **13**(5), P. 565–573.
- [22] Raveendran K. Pyrolysis characteristics of biomass and biomass components. *Fuel*, 1996, **75**(8), P. 987–998.
- [23] Fu P., Hu S., Xiang J., Sun L., Su S., and An S. Study on the gas evolution and char structural change during pyrolysis of cotton stalk. *J Anal Appl Pyrolysis*, 2012, **97**, P. 130–136.
- [24] Sing K.S.W. Reporting physisorption data for gas/solid systems with special reference to the determination of surface area and porosity (Recommendations 1984). *Pure and Applied Chemistry*, 1985, **57**(4), P. 603–619.
- [25] Thommes M. et al. Physisorption of gases, with special reference to the evaluation of surface area and pore size distribution (IUPAC Technical Report). *Pure and Applied Chemistry*, 2015, **87**(9–10), P. 1051–1069.
- [26] Schütter C., Pohlmann S., and Balducci A. Industrial Requirements of Materials for Electrical Double Layer Capacitors: Impact on Current and Future Applications. *Adv Energy Mater.*, 2019, **9**(25), P. 1900334–1900344.

- [27] Lin R., Taberna P.L., Chmiola J., Guay D., Gogotsi Y., and Simon P. Microelectrode Study of Pore Size, Ion Size, and Solvent Effects on the Charge/Discharge Behavior of Microporous Carbons for Electrical Double-Layer Capacitors. *J. Electrochem. Soc.*, 2009, **156**(1), P. A7–A12.
- [28] Nguyen H.V.T., Kwak K., and Lee K.-K. 1,1-Dimethylpyrrolidinium tetrafluoroborate as novel salt for high-voltage electric double-layer capacitors. *Electrochim Acta*, 2019, **299**, P. 98–106.

Submitted 12 January 2023; revised 8 April 2023; accepted 25 June 2023

Information about the authors:

Nguyen K. Thach – National University of Science and Technology “MISIS”, Leninskiy prospect 4, Moscow, 119049, Russia; College of electromechanical and civil engineering, Vietnam National University of Forestry, Hanoi, Vietnam; ORCID 0000-0003-3749-3198; nguyenkienthach@gmail.com

Ilya S. Krechetov – National University of Science and Technology “MISIS”, Leninskiy prospect 4, Moscow, 119049, Russia; ORCID 0000-0002-3879-8017; ilya.krechetov@misis.ru

Valentin V. Berestov – National University of Science and Technology “MISIS”, Leninskiy prospect 4, Moscow, 119049, Russia; ORCID 0000-0002-5158-1963; vberestov97@gmail.com

O. I. Kan – National University of Science and Technology “MISIS”, Leninskiy prospect 4, Moscow, 119049, Russia; ORCID 0009-0000-6057-6632; m2106915@edu.misis.ru

Ivan A. Maslochenko – National University of Science and Technology “MISIS”, Leninskiy prospect 4, Moscow, 119049, Russia; ORCID 0009-0000-2481-2976; maslochenko3@mail.ru

Tatyana L. Lepkova – National University of Science and Technology “MISIS”, Leninskiy prospect 4, Moscow, 119049, Russia; ORCID 0000-0002-0648-411X; lepkova.tl@misis.ru

Svetlana V. Stakhanova – National University of Science and Technology “MISIS”, Leninskiy prospect 4, Moscow, 119049, Russia; Mendeleev University of Chemical Technology of Russia, Miusskaya square 9, Moscow, 125047, Russia; ORCID 0000-0002-3397-9556; stakhanova.s.v@muctr.ru

Conflict of interest: the authors declare no conflict of interest.